# Anion Composition Control and Magnetic Short- and Long-Range Order in Transition Metal Oxide Hydrides

A. Bowman, J. B. Claridge, and M. J. Rosseinsky*

*Department of Chemistry, The University of Liverpool, Liverpool L69 7ZD, United Kingdom*

*Received January 25, 2006. Revised Manuscript Received April 24, 2006*

Lanthanide transition metal oxide hydride phases, $LnSrCoO_{3+\alpha}H_{\beta}$ (Ln = Pr, Nd), with variable H and O content, have been prepared by topotactic reduction of the parent $n = 1$ Ruddlesden−Popper phase, $LnSrCoO_4$, with $CaH_2$ via a $LnSrCoO_{3.5}$ ($Co^{2+}$) intermediate. The hydride anions occupy the site bridging the cations along the shorter in-plane direction in the CoOH plane. Substitution of oxide for hydride anions is incomplete leading to the compositions $NdSrCoO_{3.084(4)}H_{0.796(3)}$ (**A**), $NdSrCoO_{3.210(3)}H_{0.580(6)}$ (**B**), and $PrSrCoO_{3.160(4)}H_{0.680(7)}$ (**E**) as determined by Rietveld refinement using powder neutron diffraction data. Diffraction, thermal gravimetry, and X-ray absorption spectroscopy show that the Co oxidation state remains close to +2 despite variation in hydride content. Variable temperature neutron powder diffraction studies show that the lanthanide size and H content strongly influence the Néel temperature (410 K (**A**), 375 K (**B**), and 445 K (**E**)). All the materials are antiferromagnets. Magnetic short-range order (SRO) has also been observed, in the case of $NdSrCoO_{3.210(3)}H_{0.580(6)}$ (**B**) the SRO is two-dimensional and persists above 440 K. Correlation lengths of ∼100 Å indicate strong in-plane exchange interactions in the CoOH layers.

## Introduction

The properties of transition metal oxides are controlled by the occupancy of the d orbitals and the covalency of the cation−anion interaction. This is particularly clear in the electronic and magnetic properties of the colossal magnetoresistive manganates and high-temperature superconducting cuprates, where changes in the charge reservoir layers separating the electronically active transition metal layers tune the d-band filling to permit metal−insulator transitions with spectacular property changes. Mixed anion transition metal solids offer the opportunity to control the properties via substitution on the anion rather than the cation sublattice. Oxide nitride,[1] oxide sulfide,[2,3] and oxide halide[4,5] materials are all well established, with examples of control of properties by variation of the ratio of the two anions. It is, therefore, important to develop chemistry to allow access to new classes of mixed anion solids. Given the similarity in size of hydride ($H^-$) and halide, it is reasonable to expect that oxide hydrides will be structurally stable. However, existing classes of mixed anion solid are made by high-temperature reactions which are not suitable for the strongly reducing hydride anion—under such conditions, transition metal-containing systems would be difficult to access because of reduction to the metal by $H^-$. It has recently been shown that low-temperature syntheses in which the cation array remains unchanged during the introduction of hydride into an oxide array allow access to transition metal oxide hydrides.[6] The synthesis of these oxide hydride phases involves topotactic reduction of the layered Co(III) oxide precursor $LaSrCoO_4$ to form an intermediate anion vacancy-disordered reduced Co(II) oxide $LaSrCoO_{3.5}$[7] in which hydride substitution for oxide then takes place to afford the oxide hydride $LaSrCoO_3H_{0.7}$. The material consists of rectangular $CoOH_{1-x}$ sheets (with the hydride site ordered along the short edge of the rectangle) separated by (LaSr)O rock-salt layers (Figure 1).

Metal hydrides with both ionic and covalent contributions to bonding are known. The hydride anion in the extended transition metal oxide hydride $LaSrCoO_3H_{0.7}$ strongly influences the electronic structure of the material as a result of covalency in the metal−hydride bonding, which is confirmed by density functional theory (DFT) calculations.[8] The combined metal−oxide and metal−hydride covalency produces a magnetic ordering temperature of 380 K, which is high for a two-dimensional material, and would imply the possibility of two-dimensional magnetic correlations being present at higher temperatures as a result of the weakness of the interlayer coupling. The metal−metal separation and hydride-to-oxide ratio within the $CoOH_{1-x}$ sheets could clearly play a controlling role in the electronic properties of the resulting materials, but there is as of yet no chemistry to control this ratio. The development of the chemistry of these metastable oxide hydrides has importance beyond magnetism and correlated electron systems—the hydride anion has been

(1) Jansen, M.; Letschert, H. P. *Nature* **2000**, *404*, 980.
(2) Hyett, G.; Rutt, O. J.; Gál, Z. A.; Denis, S. G.; Hayward, M. A.; Clarke, S. J. *J. Am. Chem. Soc.* **2004**, *126*, 1980.
(3) Zhu, W. J.; Hor, P. H.; Jacobson, A. J.; Crisci, G.; Albright, T. A.; Wang, S. H.; Vogt, T. *J. Am. Chem. Soc.* **1997**, *119*, 12398.
(4) Loureiro, S. M.; Felser, C.; Huang, Q.; Cava, R. J. *Chem. Mater.* **2000**, *12*, 3181.
(5) Slater, P. R.; Gover, R. K. B. *J. Mater. Chem.* **2002**, *12* (2), 291.
(6) Hayward, M. A.; Cussen, E. J.; Claridge, J. B.; Bieringer, M.; Rosseinsky, M. J.; Kiely, C. J.; Blundell, S. J.; Marshall, I. M.; Pratt, F. L. *Science* **2002**, *295*, 1882.
(7) Hayward, M. A.; Rosseinsky, M. J. *Chem. Mater.* **2000**, *12*, 2182.
(8) Bridges, C. A.; Darling, G. R.; Hayward, M. A.; Rosseinsky, M. J. *J. Am. Chem. Soc.* **2005**, *127*, 5996.

10.1021/cm060201n CCC: $33.50 
Published on Web 06/03/2006

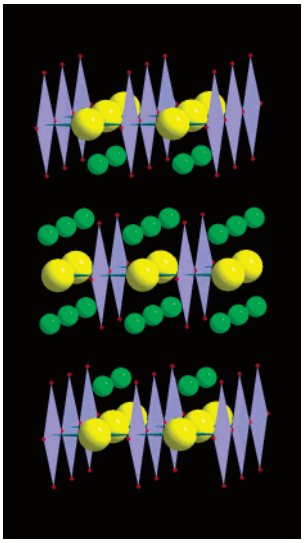

**Figure 1.** Structure of $LaSrCoO_3H_{0.7}$: $CoO_4$ squares (purple) form one-dimensional Co−O−Co chains that are connected into a rectangular layer by the hydride anions (yellow). These layers are separated by rock-salt (LaSr)O layers.

implicated in the understanding of hydrogen mobility in transition metal oxides.[9]

In this paper we show that variation of the rare earth counterion size and hydrogen pressure during synthesis allows the sheet anion compositions to be varied. The importance of the metal−hydride covalent interaction in controlling the magnetism is then demonstrated by the resulting effect of the compositional change on both the two- and three-dimensional magnetic ordering temperatures. Resolving chemically sensible local structure and global composition requires the use of a broad range of characterization techniques. As the compositional characterization involves the interplay of several techniques, the results are discussed in a sequential manner immediately after each piece of data in what follows.

## Experimental Section

**Synthesis.** *Caution:* The synthetic procedures reported here involved the buildup of hydrogen pressure in sealed tubes; eye protection must be worn, and appropriate safety measures must be taken.

Four grams of samples of $NdSrCoO_4$ and $PrSrCoO_4$ were synthesized by nitrate decomposition.[10] Dry $Nd_2O_3$ (99.99%, Alfa Aesar) or $Pr_6O_{11}$ (99.9%, Aldrich), $SrCO_3$ (99.99%, Alfa Aesar), and Co metal (99.998%, Alfa Aesar) were dissolved in dilute nitric acid. The solution was slowly heated to dryness. The mixture of nitrates was ground and then heated at 650 °C for 24 h followed by 14 h at 900 °C, 1000 °C, and 1100 °C with the sample being ground and pelletized between firings.

To prepare the oxide hydride materials, $LnSrCoO_4$ was ground together with $CaH_2$ (90−95%, Aldrich) in a 1:2 molar ratio in a He filled glovebox. Pyrex tubes were charged with the mixture and sealed under vacuum. The ampules were heated at 400 °C for 96 h (one heating cycle). These conditions were chosen after a series of initial reactions based on the in situ X-ray diffraction study discussed later allowed identification of the synthetic route required for the isolation of pure samples. Five reactions were carried out to prepare samples for neutron powder diffraction and to confirm the reproducibility of the effect of hydrogen pressure during synthesis on sample composition. The sealed tube sizes used for the Nd 3 g scale samples were 12 mm diameter × 24 cm length (**A**) and 18 mm × 19 cm (**B**), producing hydrogen pressures of 18 atm (**A**) and 9.5 atm (**B**). The Nd reactions were repeated on a 1.5 g scale with tube sizes of 12 mm × 12 cm (**C**) and 18 mm × 10 cm (**D**) producing hydrogen pressures of 17 atm and 9 atm. A 3 g Pr sample (**E**) was prepared using a tube sized 18 mm × 20 cm (hydrogen pressure 9.5 atm). In each case, after the sealed-tube reactions, the samples were washed with 0.1 M $NH_4Cl$/MeOH under $N_2$ (2 × 100 mL) to remove excess $CaH_2$ and the CaO formed in the reaction and then rinsed with dry MeOH (2 × 50 mL).

To prepare the reduced oxide, $NdSrCoO_{3.5-\delta}$, $NdSrCoO_4$ was heated under flowing 5% $H_2/N_2$ at 450 °C for 14 h and cooled to room temperature.[7]

Reaction products were characterized with Co $K\alpha_1$ radiation using a Panalytical X'Pert diffractometer equipped with an X'Celerator detector.

The structural evolution of $NdSrCoO_4$ when reacted with $CaH_2$ was studied by in situ monitoring with powder X-ray diffraction on station 9.1 at the Daresbury SRS ($\lambda = 0.8$ Å). The sample was contained in a 0.5 mm diameter capillary 4.2 cm long filled to 1.5 cm with the reaction mixture. The capillary was initially heated to 200 °C. Data were collected while the temperature was ramped from 200 to 550 °C at a rate of 0.5 °C/min. Each scan was between 13.3 and 19.7° $2\theta$ with 0.01° steps and a counting time of 1 s/step. This gave a 10 min scan duration, and the temperature, therefore, increased ∼5 °C during each scan.

**Powder Neutron Diffraction.** Neutron diffraction data were collected on $NdSrCoO_{3+\alpha}H_\beta$ (**A**) on the GEM instrument at the ISIS spallation source, Rutherford Appleton Laboratory, at 2 K, room temperature, and 393−463 K in 10 K steps. Room-temperature neutron diffraction data were collected on $NdSrCoO_{3+\alpha}H_\beta$ and $PrSrCoO_{3+\alpha}H_\beta$ (**B** and **E**) in the cryofurnace on the D2B diffractometer at the Institut Laue Langevin ($\lambda = 1.5943$ Å). Variable-temperature data were collected on the D20 instrument ($\lambda = 2.415$ Å). The samples were each heated from 1.6 K to 320 K in a cryostat at a rate of 40 °C/h. The samples were then heated in the furnace to 473 K at rates of 0.4 °C/min and 0.6 °C/min, respectively. Absorption was refined for A using a linear absorption function suitable for time-of-flight data.[11] A fixed absorption correction ($\mu R/\lambda$) was applied to the constant wavelength data collected on D2B and D20.[11,12]

**Composition.** Thermogravimetric analysis (TGA) data were collected using a Seiko SII TG/DTA 6300 instrument. The samples were heated from 25 to 800 °C under a flow of $O_2$/He with a heating rate of 5 °C/min. The gas outlet was connected to a Hiden HPR 20 RGA mass spectrometer to monitor the evolved gas-phase species ($H_2O$, $O_2$, $CO_2$, and MeOH). The $H_2O$ signal was calibrated with $CaC_2O_4 \cdot H_2O$. $PrSrCoO_{3+\alpha}H_\beta$ (**E**) was heated at 3 °C/min under a flow of 5%$H_2/N_2$.

A sample of $PrSrCoO_{3+\alpha}H_\beta$ (**E**) was prepared for transmission electron microscopy (TEM) by crushing the powder in *n*-butanol. The small crystallites in suspension were deposited onto a holey carbon film, supported by a copper grid. The TEM study was carried out with a JEOL 2000FX electron microscope. Energy dispersive

(9) Wideroe, M.; Munch, W.; Larring, Y.; Norby, T. *Solid State Ionics* **2002**, *154*, 669.
(10) Sánchez-Andújar, M.; Señarís-Rodríguez, M. A. *Solid State Sci.* **2004**, *6*, 21.
(11) Larson, A. C.; Dreele, R. B. v. *LANSCE*; Los Alamos National Laboratory, Los Alamos, 1994.
(12) Lobanov, N. N.; alte da Veiga, L. Presented at 6th European Powder Diffraction Conference, Budapest, 1998.

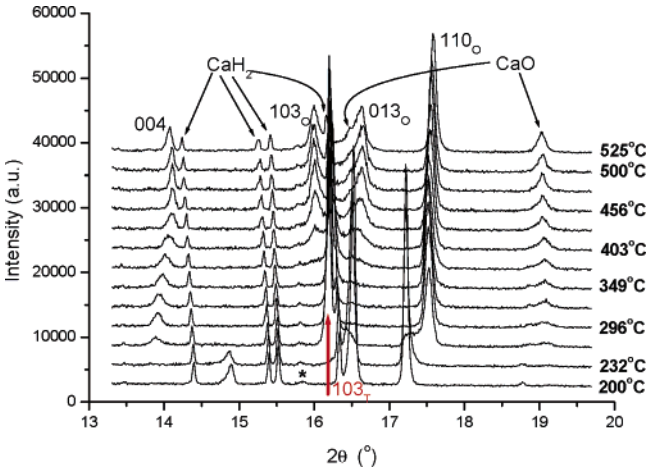


**Figure 2.** Evolution of the synchrotron X-ray diffraction pattern of an $NdSrCoO_4/CaH_2$ mixture upon heating. The temperature was increased at a rate of 0.5 °C/min from 200 to 550 °C (the capillary failed at 550 °C). Temperatures quoted are those at the end of the scan during which the temperature increased by ~5 °C. Note the reduction in the intensity of the $CaH_2$ reagent reflections, and the increased intensity of the CaO product peaks as the reaction proceeds. The formation of the oxide hydride is signaled by the observation of the splitting in the most intense reflection. The $Nd_2O_3$ impurity is marked with an asterisk (*).

spectroscopy (EDS) analyses were systematically carried out during the study, the JEOL 2000FX being equipped with an EDAX analyzer.

**X-ray Absorption Spectroscopy (XAS) Data.** XAS data were collected on station 7.1 at the SRS in ~0.5 eV steps across the Co K edge. The samples used were the Co oxidation state standards, $PrSrCoO_4$ (+3), $NdSrCoO_4$ (+3), $NdSrCoO_{3.5}$ (+2), and $La_2CoO_4$ (+2), as well as $NdSrCoO_{3+\alpha}H_\beta$ (**C** and **D**) and $PrSrCoO_{3+\alpha}H_\beta$ (**E**).

## Results and Discussion

In situ X-ray diffraction data (Figure 2) on the reaction of $CaH_2$ with $NdSrCoO_4$ indicate that the reaction proceeds via the initial formation of a tetragonal reduced oxide between 250 and 300 °C with cell parameters, $a \sim 3.7$ Å and $c \sim 13.3$ Å, indicating that this intermediate phase is similar to $NdSrCoO_{3.5-\delta}$ formed in the $H_2$ gas reduction of $NdSrCoO_4$ ($a = 3.7027(6)$ Å and $c = 13.228(2)$ Å). This is followed by the onset of orthorhombic oxide hydride phase formation at 400 °C signaled by the splitting of the $103_T$ peak of the tetragonal reduced oxide into the reflections from the orthorhombic phase ($103_O$ and $013_O$). Above 470 °C there is little change in the appearance of the pattern, and even at 525 °C the 103 and 013 peaks remain broad. The full width at half-maximum (fwhm) of the 103 peak increases from 0.07°, for $NdSrCoO_4$ at 200 °C, to 0.13°, for the orthorhombic phase at 525 °C. The breadth of the peaks may indicate a range of lattice parameters and compositions. The total duration of the experiment was 12 h. It is expected, by comparison with $LaSrCoO_3H_{0.7}$,[8] that the fwhm would reduce after heating for a longer time (i.e., days).[8] The capillary used in the in situ experiment failed when the temperature reached 550 °C.

Sealed tube reactions on bulk material confirmed that a temperature of 400 °C was necessary for oxide hydride formation, demonstrating the relationship between the reaction conditions probed by the capillary experiments and those present in bulk sample preparation. The product of an initial test reaction of $NdSrCoO_4$ with $CaH_2$ (1:2 ratio) at 350 °C for 96 h was a mixture of a tetragonal phase ($NdSrCoO_{3.5-\delta}$) and an orthorhombic phase, as has previously been observed for the La analogue.[8]

All three sets of sealed-tube reactions with calcium hydride at 400 °C produced orthorhombic materials with unit cell parameters consistent with the formation of transition metal oxide hydrides. The fwhm of the 103 peaks for the Nd materials (**A**−**D**) range from 0.09 to 0.10°, narrower than the 0.13° found at the end of the in situ experiment, as was expected after 96 h at reaction temperature, and broader than the 0.07° $NdSrCoO_4$ 103 peak (fwhm values quoted from X-ray diffraction data collected on station 9.1 at the Daresbury SRS with $\lambda = 0.8$ Å).

All the Nd compounds (**A**−**D**) contained $Nd_2O_3$ impurities originating from the starting material. No impurity phases were found in the Pr phase (**E**).

The influence of the hydrogen pressure within the tube on the orthorhombic splitting in the Nd case is reproducible, as shown by the comparison between the samples (**A** compared with **C** and **B** compared with **D**) made under the same conditions. Table 1 reveals the very similar unit cell parameters, orthorhombic strain, and out-of-plane distortion in the two samples made under each equivalent pressure. This suggests that the hydrogen pressure in the tube is the key variable in controlling the composition.

The TGA oxidation of the materials in $O_2$ (Figure 3a) permits an estimate of the hydride concentration by monitoring the quantity of evolved water by mass spectrometry. The oxygen content was determined via the total mass gain and was confirmed by reduction of the sample under hydrogen (Figure 3b). A weight gain equivalent to a composition of $PrSrCoO_{3.5}$ is observed at low temperatures in the reduction. This can be rationalized by exchange of hydride for oxide due to residual water in the reactant gas (this is further discussed in the Supporting Information). Combination of these analyses leads to the compositions given in Table 2. The Nd sample prepared at higher pressure clearly has a higher H content, and all materials display larger residual O contents than $LaSrCoO_3H_{0.7}$. The derived metal oxidation states are all similar and close to $Co^{+2}$. Data for $NdSrCoO_{3.21}H_{0.58}$ (**B**) are given in Figure S1 (Supporting Information).

This is consistent with the outcome of XAS experiments which (Figure 4, Table 3) give all the materials similar edge positions to those observed in the $Co^{II}$ standards $NdSrCoO_{3.48}$ (prepared by reduction under $H_2$ and oxygen content verified by total reduction to Co metal) and $La_2CoO_4$. The oxide hydride samples are air-sensitive and briefly exposed to air on loading onto the thermogravimetric analyzer. Adsorption of $H_2O$ during this time explains the low-temperature (~100 °C) $H_2O$ signal before the main signal, above 200 °C, which coincides with the oxidation (Figure 3a). This feature is also present in the Nd samples where the $H_2O$ signal plateaus between ~100 and 200 °C. The mass decreases before the oxidation by 0.8% and 0.2% in the case of $NdSrCoO_{3.084(4)}H_{0.796(3)}$ (**A**) and $NdSrCoO_{3.210(3)}H_{0.580(6)}$ (**B**), respectively. $Nd_2O_3$ is present in both samples (1.75(9)% (**A**) and 1.4(1)% (**B**) by mass).

**Table 1. Relationship between the Unit Cell Parameters and the Hydrogen Pressure during Synthesis at 400 °C for $LnSrCoO_{3+\alpha}H_{\beta}$ Phases[a]**

| sample label and composition | *a*, Å | *b*, Å | *c*, Å | *V*, Å$^3$ | $(a+b)/2$ | $(a+b)/c$ | $(a-b)/(a+b)$ | $H_2$ pressure, bar |
|---|---|---|---|---|---|---|---|---|
| **A**, $NdSrCoO_{3.084(4)}H_{0.796(3)}$ | 3.841(3) | 3.5585 (22) | 12.851 8) | 175.63 (15) | 3.699 75 | 0.5758 | 0.038 18 | 18 |
| **C**, $NdSrCoO_{3+\alpha}H_{\beta}$ | 3.8411(18) | 3.5576 (14) | 12.861 (9) | 175.75 (23) | 3.699 35 | 0.5753 | 0.038 32 | 17 |
| **B**, $NdSrCoO_{3.210(3)}H_{0.580(6)}$ | 3.8293(13) | 3.5718(11) | 12.931(4) | 176.86 (14) | 3.700 55 | 0.5724 | 0.034 79 | 9.5 |
| **D**, $NdSrCoO_{3+\alpha}H_{\beta}$ | 3.8302(15) | 3.5705(22) | 12.914(11) | 176.6(3) | 3.700 35 | 0.5731 | 0.035 09 | 9 |
| **E**, $PrSrCoO_{3.160(4)}H_{0.680(7)}$ | 3.8451(10) | 3.5771(11) | 12.904(4) | 177.49(12) | 3.7111 | 0.5752 | 0.036 11 | 9.5 |

[a] The compositions of **A**, **B**, and **E** as determined by powder neutron diffraction (PND). No PND data were collected on samples **C** and **D**. TGA-MS experiments confirmed the presence of $H^-$ in all phases. Tube pressure was estimated by assuming that 1 molar equiv of $CaH_2$ forms $H_2$ gas and CaO during the reaction.

**Table 2. Compositions Determined by Neutron Diffraction and TGA-MS for Samples A, B, and E[a]**

| sample (synthesis pressure) | composition (neutron diffraction) | composition (TGA-MS) |
|---|---|---|
| **A** (18 bar) | $NdSrCoO_{3.084(4)}H_{0.796(3)}$ | $NdSrCoO_{3.21(5)}H_{0.5(1)}$ |
| **B** (9.5 bar) | $NdSrCoO_{3.210(3)}H_{0.580(6)}$ | $NdSrCoO_{3.33(5)}H_{0.4(1)}$ |
| **E** (9.5 bar) | $PrSrCoO_{3.160(4)}H_{0.680(7)}$ | $PrSrCoO_{3.25(5)}H_{0.4(1)}$ |

[a] Values quoted for samples **A** and **B** from TGA-MS data do not include $Nd_2O_3$ content (after accounting for the <2% $Nd_2O_3$ found by neutron diffraction the values remain unchanged within error).

The neutron powder diffraction data collected for sample A of $NdSrCoO_{3+\alpha}H_{\beta}$ prepared under 18 atm of $H_2$ were initially analyzed using the model refined for $LaSrCoO_3H_{0.7}$.[6] Here solely hydride occupies the site bridging the cations along the shorter in-plane direction in the *ab* plane. The model was refined to the composition $NdSrCoO_3H_{0.665(8)}$. The model was modified in light of the TGA observation of excess oxygen beyond the $O_3$ composition by permitting oxide occupancy of the hydride site. The total anion occupancy of the site becomes larger than one when the O occupancy is fixed at the value obtained from the TGA (0.21) and the H occupancy is freely refined; it is clear that this is required to happen in such a model from the size of the negative scattering density at the site in the H-only refinement. As this larger than 100% occupancy of the site is not physically possible, the difference Fourier map from the H-only model was inspected (Figure 5). This revealed positive scattering density within the CoOH plane on either side of the O2 and H positions.

The positive density features around the H site can be explained by considering the need to accommodate the excess oxygen revealed by the TGA together with the large negative scattering density at the midpoint between the two Co cations along the short in-plane axis. The excess oxygen is the result of incomplete replacement of O by H during the second step of the topotactic reduction reaction from $NdSrCoO_{3.5}$ to $NdSrCoO_{3+\alpha}H_{\beta}$. The O3 oxygen occupying the hydride site needs

**Table 3. Position of Maximum of First Derivative of the Absorption Edges of $NdSrCoO_4$ (+3), $NdSrCoO_{3.48}$ (+2), Higher Pressure $NdSrCoO_{3+\alpha}H_{\beta}$ (D), Lower Pressure $NdSrCoO_{3+\alpha}H_{\beta}$ (E), $PrSrCoO_4$ (+3), $PrSrCoO_{3.16}H_{0.68}$ (C), and $La_2CoO_4$ (+2)**

| compound | position of first derivative maximum, eV |
|---|---|
| $NdSrCoO_4$ (+3) | 7722.92 |
| $NdSrCoO_{3.48}$ (+2) | 7720.88 |
| $NdSrCoO_{3+\alpha}H_{\beta}$ (~9 atm; **D**) | 7720.37 |
| $NdSrCoO_{3+\alpha}H_{\beta}$ (~17 atm; **C**) | 7720.88 |
| $PrSrCoO_4$ (+3) | 7722.91 |
| $PrSrCoO_{3.16}H_{0.68}$ (**E**) | 7720.88 |
| $La_2CoO_4$ (+2) | 7720.37 |

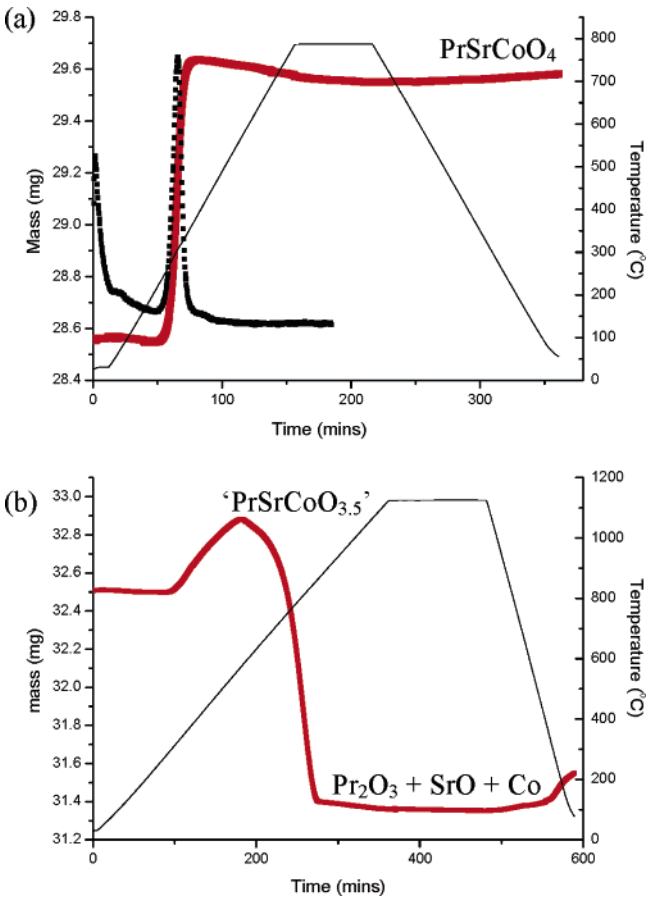


**Figure 3.** TGA of $PrSrCoO_{3.160(4)}H_{0.680(7)}$ (**E**; a) oxidation in $O_2$/He with the signal in the $H_2O$ channel of the mass spectometer overlaid (dotted line) and (b) reduction in 5% $H_2/N_2$.

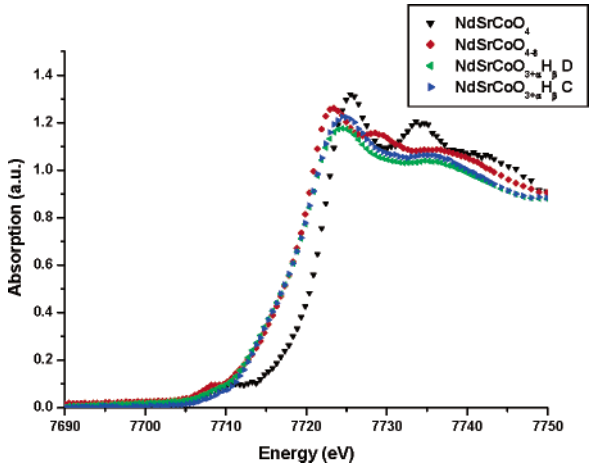


**Figure 4.** XAS data for $NdSrCoO_4$ (+3), $NdSrCoO_{3.48}$ (+2), higher pressure $NdSrCoO_{3+\alpha}H_{\beta}$ (**C**), and lower pressure $NdSrCoO_{3+\alpha}H_{\beta}$ (**D**).

**Table 4. Structural Parameters for Samples A, B, and E from Neutron Diffraction Data Collected at Room Temperature (and 2 K for $NdSrCoO_{3+\alpha}H_{\beta}$ (sample A) Only)[a]**

| | $NdSrCoO_{3+\alpha}H_{\beta}$ (**A**) | | $NdSrCoO_{3+\alpha}H_{\beta}$ (**B**) | $PrSrCoO_{3+\alpha}H_{\beta}$ (**E**) |
|---|---|---|---|---|
| | GEM: 2 K | GEM: 298 K | D2B: 298 K | D2B: 298 K |
| space group | | *Immm* | | |
| *a*, Å | 3.836 255(97) | 3.841 94(12) | 3.825 01(16) | 3.846 19(19) |
| *b*, Å | 3.552 058(93) | 3.562 47(11) | 3.569 57(16) | 3.578 25(21) |
| *c*, Å | 12.8154(3) | 12.8598(4) | 12.916 02(35) | 12.9139(4) |
| *V*, Å$^3$ | 174.631(5) | 176.009(6) | 176.351(6) | 177.730(9) |
| α | 0.084(4) | | 0.210(3) | 0.160(4) |
| *β* | 0.796(3) | | 0.581(6) | 0.680(7) |
| Ln/Sr (0, 0, *z*) *z* | 0.643 86(7) | 0.643 67(9) | 0.644 08(10) | 0.644 32(15) |
| O1 (0, 0, *z*) *z* | 0.829 74(11) | 0.829 69(15) | 0.830 11(16) | 0.829 76(16) |
| O2 (0, *y*, $^1/_2$) *y* | 0.5393(10) | 0.5451(12) | | |
| O3 (*x*, $^1/_2$, 0) *x* | 0.885(10) | 0.865(13) | | |
| moment, $\mu_B$ | 2.62(3) | 2.50(4) | 1.58(6) | 1.96(5) |
| weight fraction $Nd_2O_3$ | 1.75(9)% | | 1.4(1)% | |
| wRp | 0.0317 | 0.0397 | 0.0206 | 0.0271 |
| Rp | 0.0301 | 0.0338 | 0.0161 | 0.0216 |
| $\chi^2$ | 4.31 | 2.45 | 2.47 | 2.02 |

[a] The $Nd_2O_3$ weight fraction, α, and *β* for $NdSrCoO_{3+\alpha}H_{\beta}$ (sample **A**, $NdSrCoO_{3.084(4)}H_{0.796(3)}$) were refined using data collected at 2 K and fixed for the refinement using room-temperature data. Sample **E** ($PrSrCoO_{3.160(4)}H_{0.680(7)}$) is single phase. Sample **A** is refined with a more complex structural model, involving disordered oxygen positions O2 and O3 as described in the text. In both models Co and H have coordinates (0, 0, 0) and (0, $^1/_2$, 0). Atom site labels are given in Figure 8.

**Table 5. Isotropic (Sample A at 2 K and 298 K) and Anisotropic (Samples B and E at 298 K) Atomic Displacement Factors × 100, Å$^2$**

| | **A**, $NdSrCoO_{3.084(4)}H_{0.796(3)}$ | | **B**, $NdSrCoO_{3.210(3)}H_{0.581(6)}$ | | | **E**, $PrSrCoO_{3.160(4)}H_{0.680(7)}$ | | |
|---|---|---|---|---|---|---|---|---|
| | $U_{iso}$ | | $U_{11}$ | $U_{22}$ | $U_{33}$ | $U_{11}$ | $U_{22}$ | $U_{33}$ |
| atom | 2 K | 298 K | 298 K | 298 K | 298 K | 298 K | 298 K | 298 K |
| Ln/Sr | 0.062(11) | 0.896(22) | 1.03(9) | 1.16(10) | 1.23(8) | 1.48(13) | 1.00(15) | 1.44(13) |
| Co | 0.74(9) | 1.78(13) | 1.0(4) | 0.31(34) | 0.74(31) | 1.23(42) | 0.23(41) | 0.66(34) |
| O1 | 0.957(35) | 1.97(4) | 2.51(11) | 2.92(15) | 1.31(13) | 2.27(12) | 3.30(17) | 0.55(12) |
| O2 | 0.280(50) | 0.82(7) | 1.71(19) | 4.99(26) | 1.93(17) | 1.19(19) | 4.55(29) | 1.33(19) |
| O3/H | 2.25(15) | 3.23(21) | 0.8(4) | 0.8(4) | 0.8(4) | 1.30(34) | 1.30(34) | 1.30(34) |

**Table 6. Bond Lengths for Samples A, B, and E and Angles for Sample A ($NdSrCoO_{3.084(4)}H_{0.796(3)}$ Split Site Model)[a]**

| | $NdSrCoO_{3.084(4)}H_{0.796(3)}$, **A** | | $NdSrCoO_{3.210(3)}H_{0.581(6)}$, **B** | $PrSrCoO_{3.160(4)}H_{0.680(7)}$, **E** |
|---|---|---|---|---|
| bond lengths (Å) | 2 K | RT | RT | RT |
| Co−O1 | 2.1819(14) | 2.1902(19) | 2.1943(20) | 2.1984(21) |
| Co−O2 | 1.923 20(26) | 1.9277(4) | 1.912 50(8) | 1.923 10(9) |
| Co−O3 | 1.830(10) | 1.855(14) | 1.784 79(8) | 1.789 12(11) |
| Co−H | 1.776 03(5) | 1.781 24(6) | 1.784 79(8) | 1.789 12(11) |
| Ln/Sr−O1 | 2.3822(17) | 2.3922(23) | 2.4029(26) | 2.3948(31) |
| | 2.635 89(21) | 2.642 04(29) | 2.637 09(30) | 2.647 88(34) |
| Ln/Sr−O2 | 2.4651(25) | 2.4574(31) | 2.5784(9) | 2.5835(14) |
| | 2.6587(26) | 2.6805(32) | | |
| Ln/Sr−O3 | 2.363(25) | 2.319(31) | 2.6684(9) | 2.6780(14) |
| Ln/Sr−H | 2.6605(6) | 2.6652(8) | 2.6684(9) | 2.6780(14) |

| bond angle (deg) | 2 K | RT |
|---|---|---|
| Co−O2−Co | 171.67(21) | 170.43(26) |
| Co−O3−Co | 152.2(24) | 147.5(30) |
| Co−H−Co | 180 | 180 |
| O2−Co−O2 | 171.67(21) | 170.43(26) |
| O3−Co−O3 | 152.2(24) | 147.5(30) |
| O2−Co−H | 85.84(11) | 85.21(13) |
| O2− Co−O3 | 108.1(12) | 111.0(15) |
| | 99.7(12) | 101.5(15) |

[a] O2−Co−O2, O2−Co−H, and O3−Co−O3 angles in **B** and **C** are 180° because of the simpler structural model used. The angle H−Co−H is 180° for all three samples.

to be displaced away from the hydride position to produce a Co−O distance that is longer than the Co−H distance and is thus physically acceptable. The O3 site is, therefore, displaced perpendicular to the Co−Co vector in the refined model.

The excess density around the main oxygen site, O2, can then be accounted for as positional disorder of the O2 site produced by displacements driven by the presence of defect oxide on the H site, producing local deviation of the Co−O−Co angles from 180°. The adjusted model consists of two in-plane O sites, O2 and O3, both of which are displaced from high-symmetry positions on mirror planes and are thus disordered. O3 refines to be displaced further from the H site (0, $^1/_2$, 0) than O2 is from ($^1/_2$, 0, 0). This improves the fit ($\chi^2$ falls from 4.66 for the H-only model to 4.31 when a

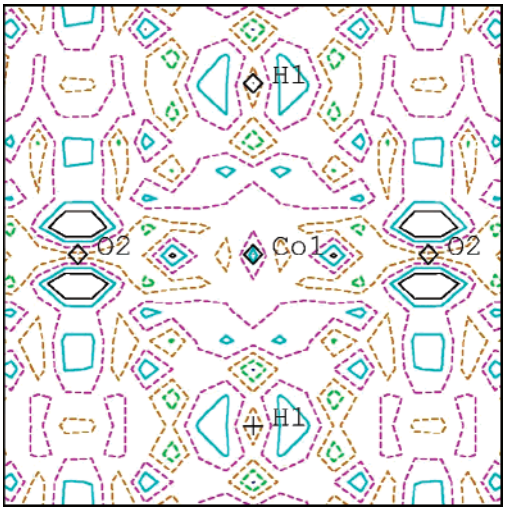


**Figure 5.** Difference Fourier map from the H-only model for the structure of sample **A** $NdSrCoO_{3+\alpha}H_{\beta}$ (backscattering bank, GEM 2 K data). The contours show the remaining negative (dotted) and positive scattering density scaled from $-3 \times 10^{-3}$ to $3 \times 10^{-3}$ ($-3 \times 10^{-3}$ shown in green, $-1.5 \times 10^{-3}$ in brown, 0 in purple, $+1.5 \times 10^{-3}$ in blue, and $+3 \times 10^{-3}$ in black). On this scale the fully occupied oxide site has a peak scattering density of 1. The centers of the blue contours on either side of H and the black contours on either side of O2 were used as the initial positions for the split O3 and O2 sites.

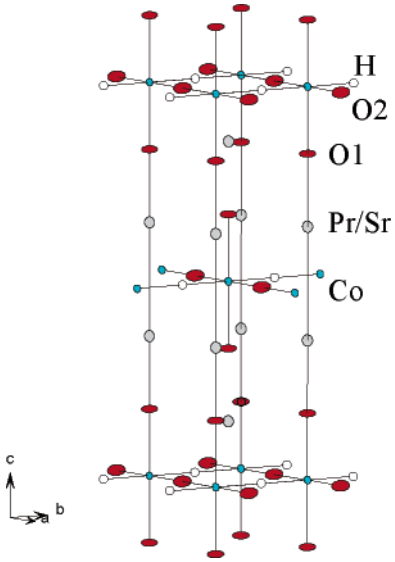


**Figure 6.** Unit cell of $PrSrCoO_{3.160(4)}H_{0.680(7)}$. Grey ellipsoids represent Pr/Sr, blue Co, red O, and white H. Atomic displacement ellipsoids are drawn with probability factor 70%. The O3 site produced by incomplete hydride substitution is not shown.

combination of hydride and displaced oxide occupy the site for the data collected at 2 K; Figure S2, Supporting Information). Isotropic atomic displacement parameters were used as the introduction of anisotropic displacement parameters caused the refinement to become unstable. The refined O3 occupancy of approximately 0.08 is necessary for the O/H site occupancy to be less than 1 and the Co oxidation state to be not greater than +2. This gives an overall composition of $NdSrCoO_{3.084(4)}H_{0.796(3)}$ with a formal Co oxidation state of +1.96 and thus agrees with the XAS data, which suggest a Co oxidation state close to +2. This composition was then fixed for the variable-temperature refinements. The refined composition differs by 0.12 oxygen per formula unit from that measured in the TGA data: detailed analysis of high-resolution X-ray powder data indicates that a second orthorhombic phase is present at the 2.6(1) wt % level. This phase may contain more oxygen, corresponding to a lower degree of hydride substitution from the $NdSrCoO_{3.5}$ starting material as it shows a smaller orthorhombic distortion ($(a - b)/(a + b) = 0.020$ for this minority phase, compared to 0.037 for the main phase in **A** and 0.035 for the lower pressure samples **B** and **E**). There is also the possibility of oxidation of the sample during loading into the thermogravimetric analyzer. However, it should be noted that the estimated standard deviations (esd's) from Rietveld refinement[11] are generally held to be significant underestimates of the uncertainty in refined parameters.[13,14] The difference may, therefore, be within the true error. It is important to note that inspection of the variance−covariance matrix indicated that there was no correlation between the occupancy of the O3 and H sites and the displacement parameters for these sites.

Refinement of the D2B and D20 data for samples **B** and **E** (which do not extend to as short *d* spacings as the GEM data for sample **A**) was not possible with the split site model. Instead the disordered O/H occupancy of the anion site bridging the shorter Co−Co distance was modeled by refining the occupancy of both species on the site with the Co oxidation state fixed at +2 as required by the XAS data. Anisotropic displacement parameters were introduced to model the O2 disorder ($\chi^2$ falls from 2.66 and 2.28 to 2.47 and 2.02 for the Nd (**B**) and Pr (**E**) compounds, respectively). O3/H atomic displacement parameters were kept isotropic and were constrained to be equal to prevent the refinement from diverging. A correlation is observed between the constrained isotropic displacement parameters and the occupancies of O3 and H, indicating that the quoted esd's are significant underestimates as the parameters are no longer truly independent.[13,14] This is probably due to the lower resolution of the D2B data at small values of *d* and the smaller number of peaks used (D2B $d_{min} = 0.83$ compared with GEM $d_{min} = 0.45$). As shown in Figure 6, the O2 displacement ellipsoids are elongated perpendicular to the Co−O2 bond in the *ab* plane. The initial analysis in terms of sole H occupancy of the (0, $^1/_2$, 0) site gave refined compositions of $NdSrCoO_3H_{0.243(8)}$ and $PrSrCoO_3H_{0.43(1)}$, that is, compositions indicating a lower hydride content than in the higher pressure synthesis for sample **A**. Both these systems thus refine to have lower hydrogen contents than the higher-pressure Nd phase, consistent with the result of the TGA-MS experiments. Incorporation of the extra oxygen indicated by the TGA data plus the compositional constraint discussed for the refinement of the GEM data above gives the compositions $PrSrCoO_{3.160(4)}H_{0.680(7)}$ and $NdSrCoO_{3.210(3)}H_{0.580(6)}$. Structural parameters and atomic displacement factors determined by powder neutron diffraction are reported in Tables 4 and 5.

EDS analyses were carried out on crystallites of both $PrSrCoO_4$ and $PrSrCoO_{3.160(4)}H_{0.680(7)}$ and led to the same average cationic composition (33.2:33.7:33.1 average ratio of Pr(L)/Sr(K)/Co(K) from eight crystallites of $PrSrCoO_{3.160(4)}H_{0.680(7)}$ (**E**)). No evidence of inhomegeneity or the presence of a nondiffracting phase was observed in

(13) Berar, J. F.; Lelann, P. *J. Appl. Crystallogr.* **1991**, *24*, 1.
(14) McCusker, L. B.; Dreele, R. B. V.; Cox, D. E.; Louër, D.; Scardi, P. *J. Appl. Crystallogr.* **1999**, *32*, 36.

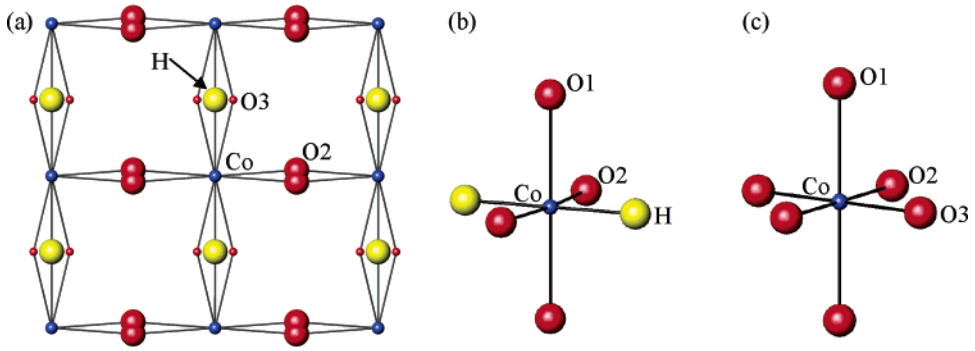


**Figure 7.** Co environment in $NdSrCoO_{3.084(4)}H_{0.796(3)}$ (sample **A**). (a) The *ab* plane with the size of the anions representing occupancy of the site; (b and c) the local Co environments corresponding to the refined average structures when the anion site on the short axis within the plane is occupied by hydride (b) or oxide (c). Co is shown in blue, O is shown in red, and H is shown in yellow.

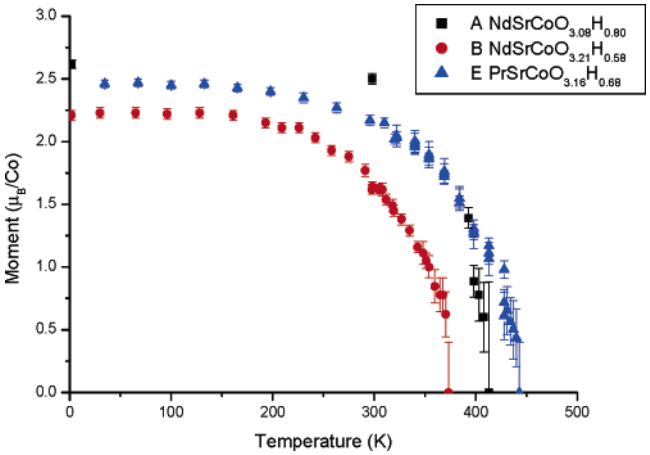


**Figure 8.** Temperature dependence of the staggered magnetic moment refined at the Co site in $NdSrCoO_{3.084(4)}H_{0.796(3)}$ (**A**), $NdSrCoO_{3.210(3)}H_{0.580(6)}$ (**B**), and $PrSrCoO_{3.160(4)}H_{0.680(7)}$ (**E**). Moments of samples B and E were set to 0 when only a broad feature is observed in the $2\theta$ range 25−37°, that is, when the sharp Bragg diffraction peaks due to three-dimensional LRO disappear.

the reduced phase, indicating that the material remains completely crystalline during the successive reactions to form reduced oxide and oxide hydride.

The Co environments in the higher pressure Nd sample, $NdSrCoO_{3.084(4)}H_{0.796(3)}$ (**A**), refined with split O2 and O3 positions, are shown in Figure 7. The displacement of O3 from the hydride site is much greater than O2 from its high-symmetry position.

The bond lengths do not vary extensively between the three compounds studied (Table 6). The smaller *b* parameter in the case of the higher-pressure Nd sample is due to the greater extent of H for O substitution, which also gives the material a smaller average unit cell volume. The Pr sample has longer bond lengths than the Nd material of equivalent composition simply as a result of ionic size and tolerance factor effects. The temperature dependence of the unit cell parameters for $NdSrCoO_{3.21}H_{0.58}$ (**B**) and $PrSrCoO_{3.160(4)}H_{0.680(7)}$ (**E**) are given in Figure S4 (Supporting Information).

All three samples showed magnetic Bragg diffraction at room temperature. A separate magnetic phase with *P*1 symmetry (cell parameters given in the caption to Figure 9) was refined for each sample on the basis of the magnetic structure of $LaSrCoO_3H_{0.7}$.[6] Below room temperature the magnitude and orientation of the moment, constrained so that neighboring Co moments are antiparallel and equal in magnitude, were refined freely. Magnetic moments of 2.50(4) $\mu_B$, 1.58(6) $\mu_B$, and 1.96(5) $\mu_B$ were obtained for $NdSrCoO_{3.084(4)}H_{0.796(3)}$, $NdSrCoO_{3.210(3)}H_{0.580(6)}$, and $PrSrCoO_{3.160(4)}H_{0.680(7)}$, respectively, at room temperature. Above room temperature the moment was fixed, and the fractional occupancy of the Co was refined and used to scale the magnetic moment. This was necessary as near $T_N$ the moment is difficult to refine because of a broad feature beneath the two most intense magnetic Bragg reflections.

The variable temperature neutron diffraction data shows a pronounced difference in magnetic ordering behavior between the Pr and the Nd low-pressure phases (Figure 8). $NdSrCoO_{3.210(3)}H_{0.580(6)}$ (**B**) displays a three-dimensional Neel temperature of 375 ± 5 K, whereas $PrSrCoO_{3.160(4)}H_{0.680(7)}$ (**E**) orders three-dimensionally at 445 ± 5 K. The higher pressure Nd phase, $NdSrCoO_{3.084(4)}H_{0.796(3)}$ (**A**), has a Neel temperature of 410 ± 5 K.

In both $NdSrCoO_{3.210(3)}H_{0.580(6)}$ (**B**) and $PrSrCoO_{3.160(4)}H_{0.680(7)}$ (**E**), the neutron diffraction data display broad features well above the disappearance of three-dimensional magnetic ordering. The broad features can be seen in Figure 9 as residual intensity in the vicinity of the 100 magnetic Bragg reflections persisting to above the three-dimensional ordering temperature. Together with the disappearance of the 101 and 012 out-of-plane magnetic Bragg reflections this suggests that two-dimensional ordering in the *ab* plane persists to temperatures above the three-dimensional ordering transition. The position of the diffuse peak corresponds to the (10) reflection of a two-dimensional square lattice and suggests that the G-type structure persists within the layer with antiferromagnetic correlations with the next nearest neighbors. These features were not observed in the time-of-flight neutron data collected on the high-pressure Nd phase **A**, $NdSrCoO_{3.084(4)}H_{0.796(3)}$, because of the poorer signal-to-noise ratio in this *Q* range in time-of-flight experiments.

For $NdSrCoO_{3.210(3)}H_{0.580(6)}$ (**B**), the broad feature displays the characteristic Warren function[15] peak shape of two-dimensionally correlated magnetic systems. The correlation length was determined by fitting the magnetic scattering[16] in the region $15° \leq 2\theta \leq 35°$ to eq 1, which combines a Warren-type line shape ($I_W(2\theta)$; eq 2) and a Lorentzian broadened nuclear reflection ($I_L(2\theta)$) with a sloping background ($A + B(2\theta)$).[16] The correlation length $\xi$ appears

(15) Warren, B. E. *Phys. Rev. B* **1941**, *59*, 693.
(16) Ahn, K.; Kremer, R. K.; Simon, A. *J. Phys.: Condens. Matter* **2004**, *16*, S875.

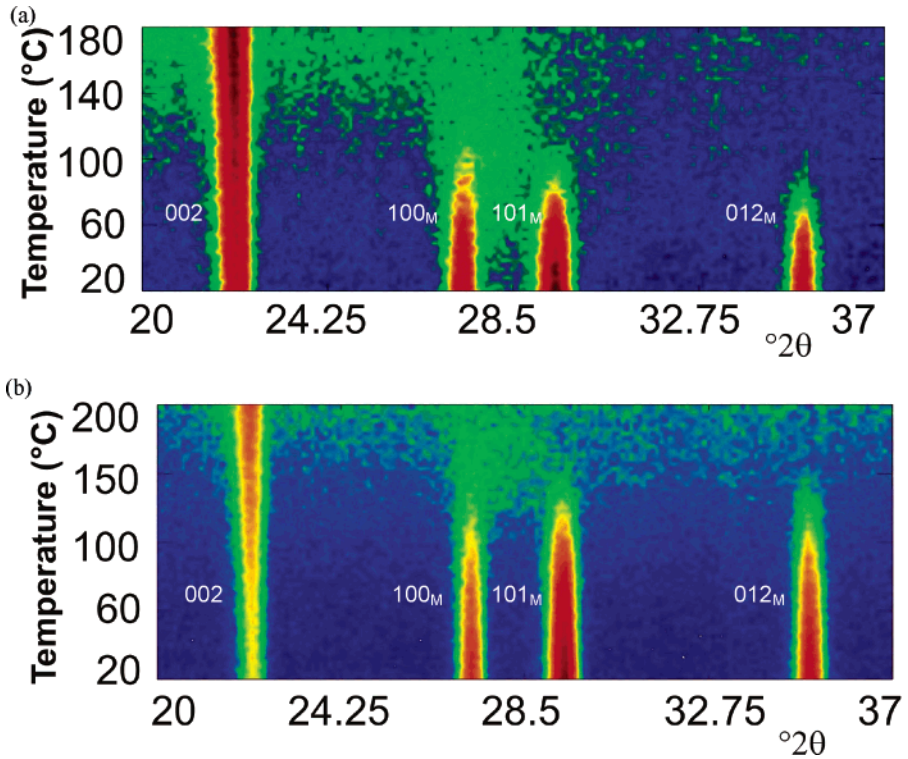


**Figure 9.** Evolution of the neutron powder diffraction patterns, collected using the D20 instrument, with temperature for (a) $NdSrCoO_{3.210(3)}H_{0.580(6)}$ (**B**) and (b) $PrSrCoO_{3.160(4)}H_{0.680(7)}$ (**E**), showing the disappearance of the magnetic Bragg peaks and the residual intensity at ~28° $2\theta$ above the three-dimensional ordering temperature. The magnetic unit cell is larger than the nuclear unit cell with $a' = b' = 5.235$ Å, $c' = 12.924$ Å, and $\gamma = 93.987°$ for $NdSrCoO_{3.210(3)}H_{0.580(6)}$ and $a' = b' = 5.255$ Å, $c' = 12.921$ Å, and $\gamma = 94.145°$ for $PrSrCoO_{3.160(4)}H_{0.680(7)}$.[6,8] The 002 nuclear peak at ~22° $2\theta$ is also plotted and increases in intensity with temperature.

temperature independent in the 375−400 K range (80 ± 20 Å; Figure 11) and then decreases. The two-dimensional correlations then become sufficiently weak that no diffuse scattering can be refined above 450 K.

$$I_{mag}(2\theta) = I_W(2\theta) + I_L(2\theta) + A + B2\theta \quad (1)$$

$$I_W(2\theta) = I_{W0}f^2(Q)\frac{1+\cos^2(2\theta)}{2(\sin(\theta))^{3/2}}\left(\frac{\xi}{\sqrt{\pi}\lambda}\right)^{1/2}F(a) \quad (2)$$

where

$$a = \frac{2\xi\sqrt{\pi}}{\lambda}(\sin\theta - \sin\theta_{W0}) \quad (3)$$

and $F(a)$ is described in the original paper by Warren.[15]

The non-Bragg scattering above $T_N$ from $PrSrCoO_{3.160(4)}H_{0.680(7)}$ (**E**) showed no obvious asymmetry and was fitted with a Lorentzian line shape (eq 4). Although this is indicative of a three-dimensional component to the correlations, it should be noted that the counting statistics in these data in this region were poorer than in the case of $NdSrCoO_{3.210(3)}H_{0.580(6)}$. The apparent difference in line shape may simply reflect this. A three-dimensional correlation length of 20 ± 10 Å, persisting up to 475 K, was determined by fitting to eq 4. The persistence of magnetic short-range order (SRO) above the three-dimensional ordering temperature is clearly established in both $NdSrCoO_{3.210(3)}H_{0.580(6)}$ and $PrSrCoO_{3.160(4)}H_{0.680(7)}$.

$$I(Q) = I_b + mQ + \frac{A}{(Q-Q_0)^2 + (1/\xi^2)} \quad (4)$$

Inspection of the data in the three-dimensionally ordered structure below $T_N$ reveals that the broad features due to the SRO persist when the Bragg scattering from magnetic long-range order (LRO) is observed (Figure S5; Supporting Information). The coexistence of broad features representing short-range correlations and three-dimensional Bragg scattering due to magnetic LRO is unusual. Coexistence of two-dimensional SRO and three-dimensional LRO has previously been reported by Knee et al. in their study of $Sr_2CoO_3Cl$.[17] $Sr_2CoO_3Cl$ has a Neel temperature of 330(5) K. Above 200 K a broad asymmetric feature, arising from two-dimensional short-range correlations, was observed. These authors suggest that stacking faults along the *c* axis or the intergrowth of closely related phases may disrupt the interlayer order, hindering the transition from three-dimensional LRO to two-dimensional SRO in some areas of the sample.[17] In the case of $LnSrCoO_{3+\alpha}H_\beta$ (Ln = Nd, Pr), unit-cell level inhomogeneity of the samples, caused by variation of the fractional occupancies of O and H anions, as indicated by both compositional measurement and structure refinement, may have a similar effect on the transition. A fluctuation in hydride content within the sample will give a spread of local exchange interactions between the Co cations. This is consistent with the observed increase of the Neel temperature of $NdSrCoO_{3+\alpha}H_\beta$ when the hydride anion concentration is higher ($T_N$ increases from 375 K for $NdSrCoO_{3.210(3)}H_{0.580(6)}$ (**B**) to 410 K for $NdSrCoO_{3.084(4)}H_{0.796(3)}$ (**A**)). The three-dimensional ordering temperature of the layered transition metal oxide hydrides increases as the two-dimensional

(17) Knee, C. S.; Price, D. J.; Lees, M. R.; Weller, M. T. *Phys. Rev. B* **2003**, *68*, 174407.

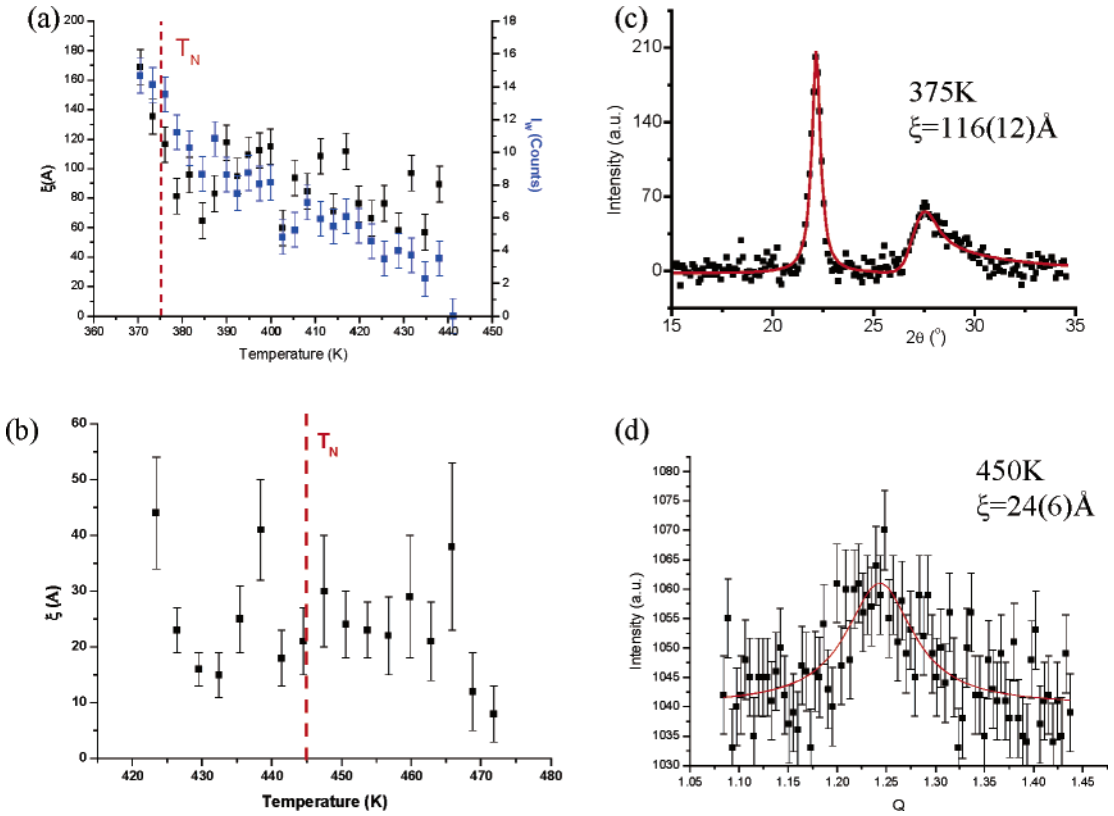


**Figure 10.** Variation of the fitted correlation length with temperature for (a) $NdSrCoO_{3.210(3)}H_{0.580(6)}$, (**B**) where a two-dimensional model was used, and (b) $PrSrCoO_{3.160(4)}H_{0.680(7)}$ (**E**), where a three-dimensional model was used. The intensity of the Warren-type peak is also plotted in part a in blue. Examples of fits to (c) the Warren-type line shape (sample **B**) and (d) the Lorentzian line shape (sample **E**) are shown. The broad feature persists to a higher temperature than the maximum measurement temperature for $PrSrCoO_{3.160(4)}H_{0.680(7)}$.

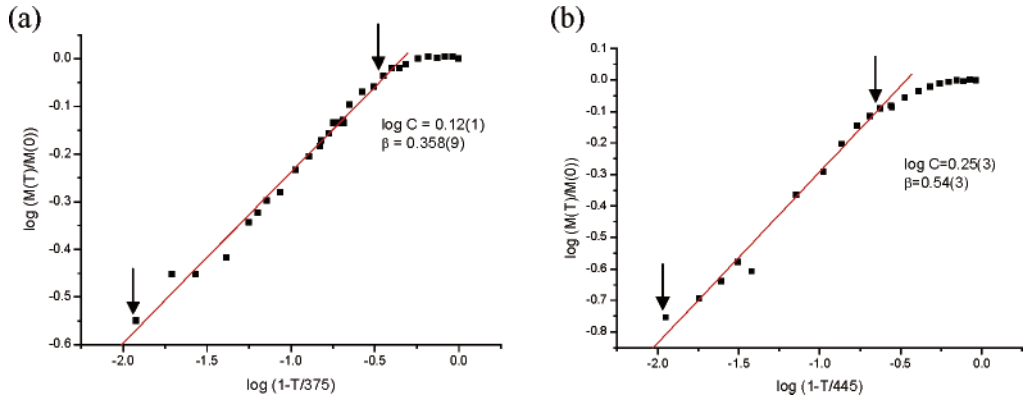


**Figure 11.** log−log plots of the normalized magnetic moment versus the reduced temperature for (a) $NdSrCoO_{3.210(3)}H_{0.580(6)}$ (**B**) and (b) $PrSrCoO_{3.160(4)}H_{0.680(7)}$ (**E**). Arrows indicate the fitting range used to determine the critical exponents, $\beta$.

correlation length within the planes increases because of stronger exchange coupling mediated by a higher concentration of hydride anions.

The low-temperature staggered moments of 2.62(3) $\mu_B$ (2 K $NdSrCoO_{3.084(4)}H_{0.796(3)}$), 2.21(4) $\mu_B$ (35 K $NdSrCoO_{3.210(3)}H_{0.580(6)}$), and 2.46(3) $\mu_B$ (2 K $PrSrCoO_{3.160(4)}H_{0.680(7)}$) are similar to the 2.76(4) $\mu_B$ observed for $LaSrCoO_3H_{0.7}$[6] and are consistent with that expected for high-spin $Co^{2+}$ given the extent of substitutional disorder in the transition metal layer, the metal−hydride covalency, and moment reduction commonly observed due to spin fluctuations in two-dimensional systems.

The transition from LRO was further analyzed by fitting plots of $\log(M(T)/M(0))$ versus $\log[1 - (T/T_N)]$ to estimate the critical exponents, $\beta$, according to the relationship described in eq 5.[18] $T_N$ was fixed at 375 K and 445 K for $NdSrCoO_{3.210(3)}H_{0.580(6)}$ (**B**) and $PrSrCoO_{3.160(4)}H_{0.680(7)}$ (**E**), respectively. A critical exponent, $\beta$, of 0.358(9) was determined for $NdSrCoO_{3.210(3)}H_{0.580(6)}$ (**B**), consistent with a three-dimensional transition (for XY $\beta = 0.345$ and for Heisenberg $\beta = 0.367$)[18] and similar to the 0.33(5) found for $Sr_2CoO_3Cl$ by Knee et al.[17] and $\beta = 0.36(1)$ found for $LaSrCoO_3H_{0.7}$ ($T_N$ fixed and data fit over same range as **B** and **E** shown in Figure 11).[8] In all these systems, it appears that the interlayer coupling plays a significant role in the growth of the LRO. This behavior contrasts with the value of 0.54(3) obtained for $PrSrCoO_{3.160(4)}H_{0.680(7)}$ (**E**) which suggests a mean field

(18) Collins, M. F. *Magnetic Critical Scattering*; Oxford University Press: Oxford, 1989.

theory model is applicable. Examination of the correlation length variation near $T_N$ for $PrSrCoO_{3.160(4)}H_{0.680(7)}$ (**C**; Figure 10b) shows no change, within error, which is consistent with mean field theory and the value of the observed critical exponent.

$$\frac{M(T)}{M(0)} = C[1 - (T/T_N)]^{\beta} \quad (5)$$

Previous estimates of the strength of the magnetic exchange mediated by both hydride and oxide within the $CoOH_{1-x}$ layers have indicated large values of $J$.[6] This is consistent with the significant two-dimensional correlation lengths found for $NdSrCoO_{3.21}H_{0.58}$ of $\geq 100$ Å; these compare with $>200$ Å for $La_2CuO_4$[19] and 20−40 Å for single-layered cobaltate[17] and manganate[20] systems, supporting the outcome of DFT calculations showing strong Co−O and Co−H interactions within the *ab* plane and the idea that hydride-mediated $\sigma$-superexchange interactions between $Co^{2+}$ cations are comparable to the strongest metal−oxide superexchange interactions. For $NdSrCoO_{3.21}H_{0.58}$ the two-dimensional correlation length decreases to ∼60 Å before vanishing above 440 K. In $PrSrCoO_{3.16}H_{0.68}$, which has a higher three-dimensional ordering temperature, the short-range correlations persist above the highest measured temperature of 470 K, consistent with even stronger exchange interactions within the layer. In $NdSrCoO_{3.21}H_{0.58}$ (**B**) the two-dimensional correlation length increases below $T_N$ as three-dimensional order is established (Figure 10a). The interlayer exchange can be calculated using eq 6 from the two-dimensional correlation length and $T_N$ as 0.23 K, at least 2 orders of magnitude weaker than estimates of the in-plane coupling.[6]

$$k_B T_N = \left(\frac{\xi}{a}\right)^2 J_z S^2 \quad (6)$$

## Conclusion

The extent of hydride for oxide substitution in neodymium- and praseodymium-containing cobalt oxide hydrides can be controlled by the hydrogen pressure, with the Co oxidation state in the resulting materials remaining close to +2 irrespective of the O/H ratio. This can be rationalized assuming the following equilibrium (eq 7):

$$LnSrCoO_{3.5} + xH_2 \rightarrow LnSrCoO_{3.5-x/2}H_x + \frac{x}{2}H_2O \quad (7)$$

$$\Delta G = \Delta G^\circ + RT \ln {p_{H_2O}}^{x/2} - RT \ln {p_{H_2}}^{x} \quad (8)$$

The reaction will proceed when $\Delta G \leq 0$. It can be assumed that $\Delta G^\circ$ is positive (the low-temperature oxidation of the oxide hydride materials by adventitious $H_2O$ in the 1 atm, 5% $H_2/N_2$ stream in the TGA experiment before the onset of reduction (Figure 3b provides evidence for this assumption), and thus precise control of both hydrogen pressure and water partial pressure will be required to obtain reaction and, therefore, complete compositional control in this family by varying the value of $x$. In the sealed tube systems used here, the partial pressure of water is kept very low by the presence of excess $CaH_2$, which effectively getters any residual contamination. It is, therefore, unlikely that oxide hydrides could be formed in a flow system as the residual water pressure is probably too high. Mass action in eq 8 then dictates that a higher hydrogen pressure will produce a larger hydride content in the product oxide hydride, consistent with the observations here. It is important to emphasize that the equilibrium in eq 7 cannot be set up by reaction of gas-phase hydrogen and the metal oxide. The oxide hydride is formed by a solid−solid substitution reaction involving $CaH_2$, as shown by quantitative analysis of reactant phase fractions during the formation of the oxide hydride.[8] Once the hydride is introduced, it is then in equilibrium with gas-phase hydrogen, affording the compositional control. The above model also explains the need for an excess of $CaH_2$ in syntheses of the oxide hydrides; this is essential to maintain the water partial pressure at a sufficiently low value to prevent displacement of hydride by water-derived oxide.

The incomplete hydride-for-oxide substitution produces local variations in the Co coordination environment which are identified as displacements of both majority (long in-plane axis) and minority (short in-plane axis) oxide anions. The change in lanthanide size and oxide-to-hydride ratio has a dramatic effect on the magnetic properties, with three-dimensional antiferromagnetic ordering temperatures ranging from 375 K to 445 K; it should be noted that the Co(II) oxide $LaSrCoO_{3.5}$ has a Néel temperature of 180 K. Comparison of three-dimensional ordering temperatures for the two Nd phases studied suggests that hydride produces stronger superexchange interactions than oxide. The observation of SRO, which is clearly two-dimensional in the case of $NdSrCoO_{3.210(3)}H_{0.580(6)}$, persisting to beyond 440 K with correlation lengths of over 100 Å, confirms the strong in-plane exchange in the $Co^{2+}$ oxide hydride layers and that three-dimensional order is driven by the interlayer coupling which is 2 orders of magnitude weaker than the in-plane interactions. Higher three-dimensional ordering temperatures correlate with the SRO features persisting to higher temperature. The importance of the interlayer coupling in establishing LRO is significant despite being 2 orders of magnitude weaker than estimates of the in-plane exchange. The variation in hydride content and lanthanide size makes direct comparison between the magnetic behavior of the four characterized single-layered transition metal oxide hydrides difficult, but it is clear from comparison of the two neodymium phases studied here that an increase in hydride concentration produces an increased three-dimensional magnetic ordering temperature. This is qualitatively consistent with strong superexchange interactions mediated by the hydride anion.

**Acknowledgment.** The authors thank the UK EPSRC for Portfolio Partnership support. The authors thank CCLRC for access to ISIS, ILL, and SRS, and Dr. P. Henry, Dr. R.M. Ibberson, Dr. M.A. Robert,s and Dr. J.F.W. Mosselmans for assistance with experiments on the D20, GEM, 9.1, and 7.1 instruments, respectively. We also thank Dr. R.K. Kremer for providing the program used to perform the Warren function fit.

(19) Birgeneau, R. J.; Greven, M.; Kastner, M. A.; Lee, Y. S.; Wells, B. O.; Endoh, Y.; Yamada, K.; Shirane, G. *Phys. Rev. B* **1999**, *59*, 13788.
(20) Bieringer, M.; Greedan, J. *J. Mater. Chem.* **2002**, *12*, 279.

**Supporting Information Available:** TGA oxidation of sample **B**, 2 K Rietveld refinement of **A**, room-temperature Rietveld refinements of samples **B** and **E**, temperature dependence of the unit cell parameters for samples **B** and **C**, and critical exponent determination for $LaSrCoO_3H_{0.7}$ (PDF). This material is available free of charge via the Internet at http://pubs.acs.org.

CM060201N